Environmental Science & Technology

pubs.acs.org/est

Article

Direct Quantification of the Effect of Ammonium on Aerosol Droplet pH

Qishen Huang, Haoran Wei, Linsey C. Marr, and Peter J. Vikesland*

Cite This: *Environ. Sci. Technol.* 2021, 55, 778−787

Read Online

ACCESS | Metrics & More | Article Recommendations | Supporting Information

ABSTRACT: Ammonium is an important atmospheric constituent that dictates many environmental processes. The impact of the ammonium ion concentration on 10−50 μm aerosol droplet pH was quantified using pH nanoprobes and surface-enhanced Raman spectroscopy (SERS). Sample solutions were prepared by mixing 1 M ammonium sulfate (AS), ammonium nitrate (AN), sodium sulfate (SS), or sodium nitrate (SN) solutions with 1 M phosphate buffer (PB) at different volume ratios. Stable pH values were measured for pure PB, AS, and AN droplets at different concentrations. The centroid pH of 1 M PB droplets was ∼11, but when PB was systematically replaced with ammonium (AS- or AN-PB), the centroid pH within the droplets decreased from ≈11 to 5.5. Such a decrease was not observed in sodium (SS- or SN-PB) droplets, and no pH differences were observed between sulfate and nitrate salts. Ammonia partitioning to the gas phase in ammonium-containing droplets was evaluated to be negligible. Raman sulfate peak (∼980 cm^{-1}) intensity measurements and surface tension measurements were conducted to investigate changes in ion distribution. The pH difference between ammonium-containing droplets and ammonium-free droplets is attributed to the alteration of the ion distribution in the presence of ammonium.

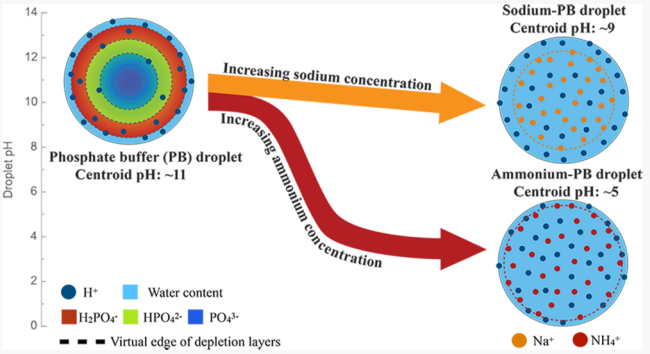

INTRODUCTION

Aerosols and droplets with high water content are important systems that dictate many atmospheric processes. For such aerosols, pH is arguably the key controlling parameter as it affects aerosol physicochemical properties (e.g., size,[2] surface tension,[3] and mixing state[4]) and ultimately impacts climate,[5] human health,[6−8] and aerosol reactivity.[9,10] Many atmospheric processes, such as sulfate aerosol formation and halogen chemistry, are pH-sensitive.[11,12] pH potentially dictates the cloud condensation nuclei (CCN) activity of atmospheric aerosols because of its correlation with ammonia and sulfate,[13] and aerosol pH can affect human health (e.g., inhalation toxicity of $PM_{2.5}$;[6] influenza virus stability in droplets and aerosols[7,8,14]). Previous studies have shown the pH dependence of liquid−liquid phase separation (LLPS) in aerosols containing organic acids and ammonium sulfate.[15,16]

Ammonium sulfate (AS) is a major component of secondary aerosols,[17,18] and AS is frequently invoked for its role in CCN formation.[19] The major pathway by which AS forms in the atmosphere is through the uptake of gaseous ammonia by acidic sulfuric acid aerosols.[5] As such, sulfuric acid plays an important role in the formation of new atmospheric particles.[20−22] As the most abundant alkaline species in the atmosphere, ammonia is significant in the heterogeneous neutralization of acidic aerosols.[23] The influence of pH on aerosol composition is often related to the atmospheric ammonia concentration.[24]

The effect of the air−water interface on aerosol composition is significant.[25] Chemical reaction rates within microdroplets can be enhanced by the interfacial accumulation of ions and the development of heterogeneous pH regions.[26,27] At the air−liquid interface, ions experience either depletion or enrichment, and the structure of interfacial water can change based upon aerosol composition.[28] For example, sodium has been suggested to be excluded from the air−water interface based on the measured increase in surface tension for elevated sodium salt concentrations.[3,29] Surface accumulation of protons, or hydronium (H_3O^+) ions, has been reported in both modeling and experimental studies.[30,31] Recently, a pH gradient from the air−water interface to the droplet centroid was observed in phosphate-buffered aerosol droplets as a result of the apparent enrichment of protons at the air−water interface.[1]

A number of approaches are used to evaluate aerosol pH. Proxy methods are frequently employed to indirectly predict aerosol pH or to validate bulk pH measurements.[32] The

Received: November 2, 2020
Revised: November 24, 2020
Accepted: November 25, 2020
Published: December 9, 2020

https://dx.doi.org/10.1021/acs.est.0c07394
Environ. Sci. Technol. 2021, 55, 778−787

accuracy of four proxy methods was recently reviewed.[33] Of the four methods, estimates based upon the phase partitioning of ammonia reportedly provided the best prediction of aerosol pH. Thermodynamic models, such as E-AIM (extended aerosol inorganics model)[34] or ISORROPIA-II,[35] provide results that agreed with the phase partitioning method while also considering gas-phase partitioning. Predictions made using the ion balance method or molar ratio method cannot accurately represent aerosol pH. Thermodynamic methods can be combined with aerosol compositions measured from field samples to approximate aerosol pH; however, perturbations during sample collection must be accounted for.[10]

Individual aerosol droplets are highly dynamic and heterogeneous,[36] and as such, they may behave quite differently from what is predicted via proxy or field sampling methods. The complex composition and variable properties of aerosols[37] demand methods that provide high temporal and spatial resolution.[4] Such demand urges the development of real-time, single particle measurements. Probe-based surface-enhanced Raman spectroscopy (SERS) can achieve single particle pH measurements. Raman spectroscopy provides chemical fingerprints of the system,[1,38] which makes the method promising for aerosol characterization and pH measurement.[10,39,40]

In this study, ammonium and sodium electrolyte concentrations were systematically varied in PB droplets. In this manner, we investigated how these ions impact droplet pH such that we could enhance our understanding of their role in atmospheric systems. The effects of the constituent type and its concentration were investigated, and the role of the air−water interface in dictating electrolyte behavior is discussed.

MATERIALS AND METHODS

Chemicals and Materials. Gold chloride trihydrate ($HAuCl_4 \cdot 3H_2O$), sodium citrate tribasic dehydrate ($Na_3citrate \cdot 2H_2O$), 4-mercaptobenzoic acid (4-MBA), and polyvinylidene fluoride (PVDF) membranes (0.22 μm pore size, 13 mm in diameter) were purchased from MilliporeSigma. Polyethylene glycol thiol (m-PEG-SH, 5 kDa) was obtained from Nanocs. AEROSILR202 (silicone oil treated hydrophobic fumed silica) was purchased from Evonik Industries. Standard solutions with known pH were prepared with phosphoric acid (H_3PO_4, 1 M) and sodium hydroxide (NaOH, 1 M) for pH probe validation. Stock solutions were prepared using sodium hydroxide (NaOH), ammonium sulfate [$(NH_4)_2SO_4$, AS], sodium sulfate (Na_2SO_4, SS), ammonium nitrate (NH_4NO_3, AN), sodium nitrate ($NaNO_3$, SN), and 1 M phosphate buffer (PB). The chemicals used for solution preparation were obtained from Fisher Scientific. All chemicals were used directly as purchased. All solution pH values were recorded using a commercial pH meter (Orion versa star pro, Thermo Scientific) after preparation. For bulk pH measurements, the stock solutions were diluted to 0.6 of their original concentration to match the final solute concentration in droplets following addition of the pH nanoprobes.

Synthesis of AuNP-Based pH Probes. SERS-active pH probes were prepared following our previously described approach: (1) synthesis of 50 nm gold nanoparticles (AuNPs) via modified seed-mediated growth[41] and (2) surface functionalization with 4-MBA and coating with m-PEG-SH.[42] In brief, 13 nm AuNPs were prepared following the method of Frens et al.[43] A 100 mL aliquot of gold precursor containing 1 mM $HAuCl_4 \cdot 3H_2O$ was pH adjusted to 6.2−6.5 with 1 M NaOH. Sodium citrate (final concentration 3.88 mM) was added to the boiling precursor under vigorous stirring. The suspension was boiled for 15 min and then cooled at room temperature. Larger 50 nm AuNPs were prepared from the 13 nm AuNPs. A 100 mL $HAuCl_4$ solution (0.254 mM) was brought to boil while being stirred, and 800 μL of seed suspension and 0.44 mL of citrate (38.8 mM) were added sequentially. The suspension was refluxed for ≈30 min and then cooled to room temperature.

To synthesize the pH nanoprobe,[42] a 10 mL aliquot of 100 μM 4-MBA in ethanol and an equivalent volume of AuNP suspension (5×10^{10} NPs/mL) were mixed together while stirred. The vessel was maintained at room temperature for 3 h until the suspension turned purple. A 2 mL aliquot of 500 μM mPEG-SH was added to the mixture, and the suspension was stirred at room temperature for another 2 h. The product was isolated by centrifugation at 3000g for 15 min and then redispersed in deionized water. As described in the Supporting Information, the products from each step were characterized using UV−vis spectroscopy and dynamic light scattering (DLS; Figure S1 and Table S1).

Generation and Collection of Aerosol Droplets. Aerosol droplets were generated from prepared stock solutions using a commercial atomizer (TSI 3076, TSI Inc.). Individual AS, AN, SS, or SN solutions of 1 M concentration were mixed with 1 M PB with the relative volume ratio ranging from 0 (100% PB) to 1 (0% PB) to generate mixtures with progressively increasing AS, AN, SS, or SN concentrations and progressively decreasing PB concentrations. A constant total salt concentration was used to minimize hygroscopicity differences between droplets as it retains a constant water activity.[44] The hygroscopicity of an aerosol droplet is at least partially dictated by its total salt concentration.[2] At the high ionic strengths involved in this study, solute concentration might need to be considered;[45] however, a fixed total solute concentration was used because it can be readily controlled, and it aids in maintaining droplet stability during pH measurements (Figure S2).

During an aerosolization experiment, the atomizer was placed in a custom chamber that maintained relative humidity (RH) at 95%. A superhydrophobic filter was prepared by coating 100 μL of AEROSIL-acetone suspension (4 g/L) onto a PVDF filter via air-drying. Samples containing 2 mL of probe suspension and 3 mL of experimental solution were aerosolized and then collected for 2 min on a superhydrophobic filter held ≈0.5 cm away from the atomizer outlet. The contact angle for droplets collected on this substrate was ≈150° (Figure S3). Following dilution, unless otherwise stated, the final salt concentration in the aerosolized droplets was 0.6 M. The filter was transferred into an imaging flow cell (FC310, BioSurface Technologies Corp.) for SERS measurements.

SERS Measurements. Single aerosol droplets were scanned using a confocal Raman microscope (WITec Alpha 500R) and a 50× objective lens and a 785 nm laser. The droplets measured in our study were 10−50 μm in diameter and were ≈25 μm on average. A typical droplet size distribution is depicted in Figure S4. Every measurement consisted of collection of a 20 × 20 pixel SERS map that represents a 50 × 50 μm^2 area that was larger than the target droplets. The laser was initially focused at the droplet centroid, and the integration time was 0.1 s for all measurements. The imaging flow cell was connected to an automatic RH controller during all droplet measurements, and the RH was maintained

https://dx.doi.org/10.1021/acs.est.0c07394
Environ. Sci. Technol. 2021, 55, 778−787

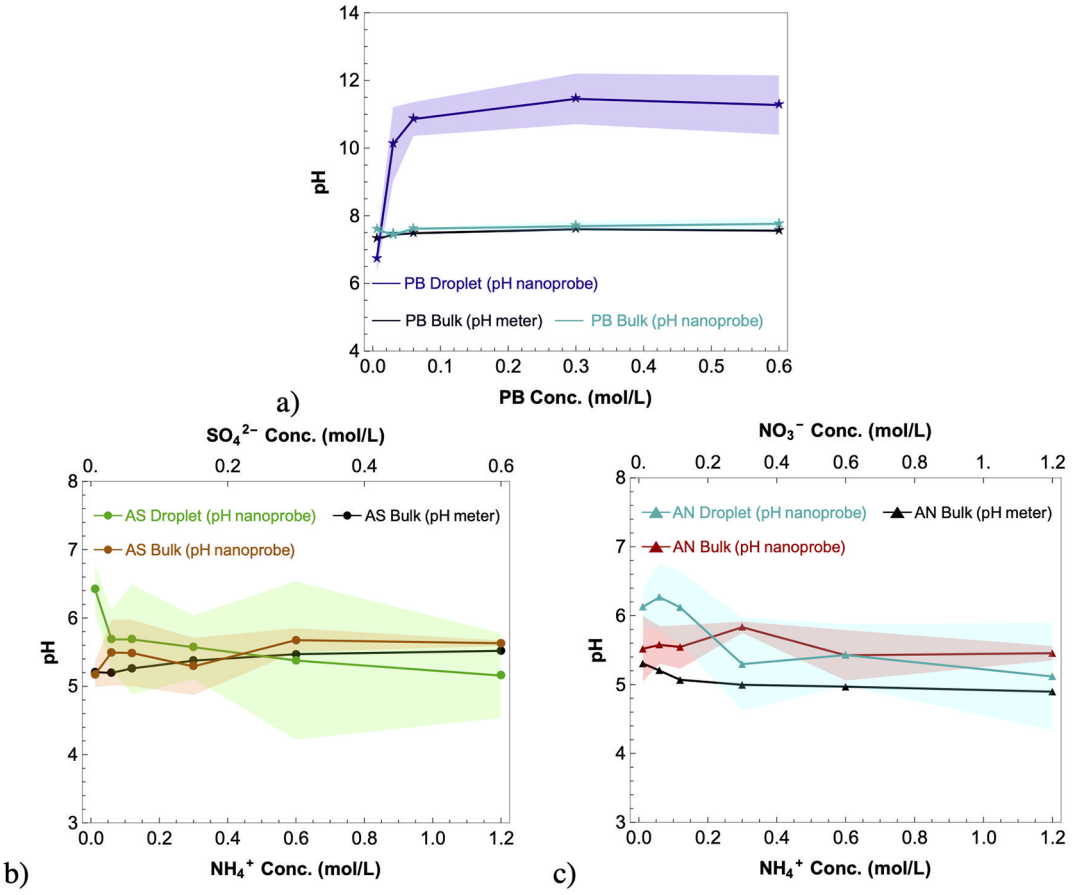

Figure 1. Measured pH of droplets vs bulk solutions for different initial solute concentrations: (a) PB; (b) ammonium sulfate; and (c) ammonium nitrate. In (b,c), the lower *x*-axis represents the ammonium concentration (M) in the stock solution prior to aerosolization and the upper *x*-axis represents the corresponding anion (sulfate/nitrate) concentration (M). The colored belts indicate the standard deviation of 15 replicate droplets at each concentration.

at 95%. Bulk solution pH values were measured in a quartz cell (Starna Cells Inc.) with the laser focused 200 μm below the upper cell wall. For bulk solution measurements, the selected scan area was 100 × 100 μm^2. All other parameters for bulk pH measurements were the same as those used for droplets.

Surface Tension Measurement. The surface tension of a selected set of solutions or suspensions was measured using a goniometer and DROPimage Advanced software (Ramé-hart). For each sample, the surface tension of three different pendent droplets (≈20 μL, 1 cm diameter) was measured. Each measurement represents an average of 20 calculation results (details about these surface tension measurements are given in the Supporting Information). Surface tension measurements were obtained using electrolyte solutions and electrolyte/nanoprobe suspensions to determine if the presence of the nanoprobe affects droplet surface tension.

Equilibrium Calculations. Equilibrium pH was calculated for bulk solutions and AS and AN droplets to assist data interpretation. The bulk solution pH was calculated using Visual MINTEQ ver. 3.1, and the pH of the droplets was estimated using E-AIM III (Table S2).[46] In the MINTEQ calculations, solution pH was calculated using mass and charge balances. Both ideal solution simulation (ionic strength fixed at 0) and more realistic simulations (calculated ionic strength via mass and charge balances) were conducted.

RESULTS AND DISCUSSION

Validation of pH Probe. Nanoprobe response to solution pH is dependent on the protonation and deprotonation of the carboxyl group of 4-MBA (pK_a = 8.75; Figure S5).[42] 4-MBA exists in its protonated form under acidic conditions, and the 1410 cm^{-1} peak intensity is reduced, while the 1710 cm^{-1} peak intensity is enhanced. To address signal variability that arises from differences in the local nanoparticle concentration, the intensities of these pH-dependent peaks were normalized to the intensity of the pH-insensitive 1076 cm^{-1} peak.[47] The pH of the scanned area was calculated using the peak ratios of 1410/1076 or 1710/1076 cm^{-1} averaged from 400 separate spectra.[1,42] Each reported pH represents the average of three independent measurements of the same sample. Figure S6 provides a comparison of solution pH values measured using a nanoprobe and commercial pH meters. The pH values measured by the nanoprobes were calculated using calibration curves developed according to our prior work.[1] In the low pH range (<4), the 1410/1076 cm^{-1} peak ratio is indistinguishable from the spectral background, while at high pH (>8), the 1710/1076 cm^{-1} peak ratio is indistinguishable. Accordingly, for all pH calculations, when the pH was <4, the pH was determined using the 1710/1076 cm^{-1} ratio and when the pH > 8, the pH was calculated using the 1410/1076 cm^{-1} ratio. Either peak ratio can be used when pH is between 4 and 8. Under pH > 12 conditions, the pH values calculated from both peak ratios deviate from the solution pH measured using a

https://dx.doi.org/10.1021/acs.est.0c07394
Environ. Sci. Technol. 2021, 55, 778−787

commercial pH meter. Considering that the standard deviation at pH = 2 is high, the sensitive detection range of the nanoprobe is approximately 3−12.

The pH of stock electrolyte solutions was measured using the pH nanoprobes and compared to the pH values measured using a commercial meter (Figure S7). Across all electrolyte compositions, independent *t*-tests indicated no significant difference between the two methods within the pH 3−12 range ($p > 0.05$). These measured pH values agree with those calculated using Visual MINTEQ ver. 3.1 (Figures S7, S8).

Effects of PB Concentration on Droplet pH. We previously reported that the pH of a bulk sample of 0.6 M PB was 7.4, but at the centroid of 10−50 μm PB droplets, the pH was ≈11.[1] Herein, we studied droplets in which we progressively reduced the PB concentration from 0.6 to 0.006 M to improve our understanding of how droplet chemistry affects pH. We again note that this reported concentration range reflects dilution of the starting solutions with nanoprobe suspension prior to aerosolization. For PB concentrations above 0.03 M, the pH of the droplets was >10 and was independent of PB concentration (Figure 1a). At a PB concentration of ≈0.006 M, the pH of the PB droplets converged with that of the bulk solution. At such low PB concentrations, the droplets were small (<10 μm) and rapidly evaporated during the course of a pH measurement. Because of the difference in hygroscopicity, droplets with lower salt concentrations evaporate more rapidly than those at higher concentrations,[2] and thus, the pH decrease measured in low concentration PB droplets may partially reflect evaporation.

One explanation for the observed elevated pH in PB droplets relative to bulk solution is that, in a pure PB droplet, protons, likely in the form of hydronium ions,[30] are enriched at the air−water interface, thus leaving the center of the droplet hydroxide-rich. Bare protons in water have the largest hydration energy among monovalent ions; thus, protons are likely to exist in their hydrated hydronium form in aqueous systems.[48] Hydronium is capable of forming complex structures with surrounding water molecules and is thought to partition closer to the air−water interface than other small cations.[30,49]

Another way to interpret the pH of PB aerosol droplets is from the perspective of bulk solution chemistry. The pH of phosphate buffer is described using either $\mathrm{pH} = \mathrm{p}K_{a2} + \log \frac{[\mathrm{HPO_4^{2-}}]}{[\mathrm{H_2PO_4^-}]}$ or $\mathrm{pH} = \mathrm{p}K_{a3} + \log \frac{[\mathrm{PO_4^{3-}}]}{\mathrm{HPO_4^{2-}}}$ depending on the pH range (Figure S9). The high centroid pH of a PB droplet suggests an increase in the $[\mathrm{HPO_4^{2-}}]/[\mathrm{H_2PO_4^-}]$ ratio and enhanced $[\mathrm{PO_4^{3-}}]$. We estimated the ratios of $[\mathrm{HPO_4^{2-}}]/[\mathrm{H_2PO_4^-}]$ and $[\mathrm{PO_4^{3-}}]/[\mathrm{HPO_4^{2-}}]$ given the $\mathrm{p}K_{a2}$ (=7.21) and $\mathrm{p}K_{a3}$ (=12.67) of phosphoric acid and the measured pH of the PB droplets. Our previous study showed that the pH of a PB droplet was ≈11 in the center and decreased gradually to ≈8 near the air−water interface.[1] This gradient suggests the relative enrichment of $\mathrm{H_2PO_4^-}$ near the air−water interface and comparatively higher amounts of $\mathrm{PO_4^{3-}}$ at the droplet center. Gradually changing ratios between the three phosphate anions should exist from the droplet interface to the centroid. Thermodynamically, electrolytes have the tendency to be depleted from the air−water interface to minimize surface energy.[50] Multiply charged inorganic anions have been reported to prefer bulk solvation as the electrostatic forces that repel anions from the interface often overwhelm surface-favoring polarization interactions.[49,51] For $\mathrm{PO_4^{3-}}$, $\mathrm{HPO_4^{2-}}$, and $\mathrm{H_2PO_4^-}$, which have charges of −3, −2, and −1, respectively, the electrostatic penalty of bringing the anion close to the surface follows the sequence: $\mathrm{PO_4^{3-}} > \mathrm{HPO_4^{2-}} > \mathrm{H_2PO_4^-}$.[52] Therefore, $\mathrm{H_2PO_4^-}$ and $\mathrm{HPO_4^{2-}}$ are more weakly repelled from the air−water interface, while $\mathrm{PO_4^{3-}}$ experiences the greatest interfacial repulsion. At the molecular level, hydrated multiply charged anions possess a stronger charge−dipole interaction with water compared to singly charged anions, and thus, multiply charged anions are often solvated in the bulk solution.[51] The enrichment of $\mathrm{H_2PO_4^-}$ closer to the air−water interface is likely due to the depletion of the two other anions. The heterogeneous distribution of the three phosphate anions in micron droplets can be regarded as an extended effect resulting from their distinct interfacial preferences. High solute concentrations could enhance this interfacial effect. Such a distribution minimizes the total energy of the system and causes the hydronium in the droplet to be enriched at the air−water interface.

Effects of AS and AN Concentration on Droplet pH. We also examined how changes in the AS and AN concentration between 1.2 and 0.012 M (as ammonium concentration) impacted droplet pH. Unlike PB droplets, whose pH values were consistently higher than that of the bulk, no apparent pH difference was observed between AS or AN droplets and their bulk solutions (Figure 1b,c). The average pH of the AS and AN droplets was between 5 and 6 when the ammonium concentration exceeded 0.06 M. Similar to PB droplets, at low AS and AN concentrations, the droplets evaporated rapidly, and the apparent change in droplet pH at low concentration may reflect this instability.

The partitioning of ammonia between the gas phase and aerosol droplets buffers pH.[53] We utilized E-AIM to evaluate liquid-to-gas ammonia partitioning. At equilibrium, the pH of AS droplets is expected to be 4.3 at 95% RH according to E-AIM. This value is within the standard deviation of our droplet pH measurements and is much lower than the $\mathrm{NH_4^+}$ $\mathrm{p}K_a$ (= 9.3). At a pH of 4.3, the ammonia concentration within an AS droplet is $\approx 7.0 \times 10^{-5}$ M and exerts a partial pressure of 1.2×10^{-6} atm. Given the high $\mathrm{p}K_a$ of ammonium, the low ammonia concentration, and its low partial pressure, we expect that partitioning of ammonia from the droplet to the gas phase should be negligible in pure AS/AN droplets.

The similar pH values determined for ammonium droplets and bulk solutions suggest that no apparent pH gradient exists in ammonium droplets and that the ions are homogeneously distributed. In the AN system, other than hydronium and hydroxide, only one type of cation ($\mathrm{NH_4^+}$) and one type of anion ($\mathrm{NO_3^-}$) are present. In AS droplets, in contrast, two types of anions ($\mathrm{SO_4^{2-}}$ and $\mathrm{HSO_4^-}$) are possibly present; however, the concentration of $\mathrm{HSO_4^-}$ can be neglected because the $\mathrm{p}K_{a2}$ of sulfuric acid is 1.99 and within the observed droplet pH range the amount of $\mathrm{HSO_4^-}$ is <0.1% of $\mathrm{SO_4^{2-}}$. Accordingly, the AS systems can be considered to contain predominantly $\mathrm{SO_4^{2-}}$. Even in the absence of a pH effect from the conjugated ions, an apparent preference of ions toward either the interface or the droplet interior would still elicit a pH difference between droplets and the bulk solution. The ammonium−water complex has a "hydronium-like" structure as the solvation shell for a single ammonium is relatively small (~2.8 Å)[54] compared to that of sulfate (~3.8 Å) or nitrate (~3.2 Å),[55] and the ammonium−water interaction is weak. Such a structure enables ammonium to diffuse relatively unhindered between hydrogen-bonded water molecules.[49,56,57]

https://dx.doi.org/10.1021/acs.est.0c07394
Environ. Sci. Technol. 2021, 55, 778−787

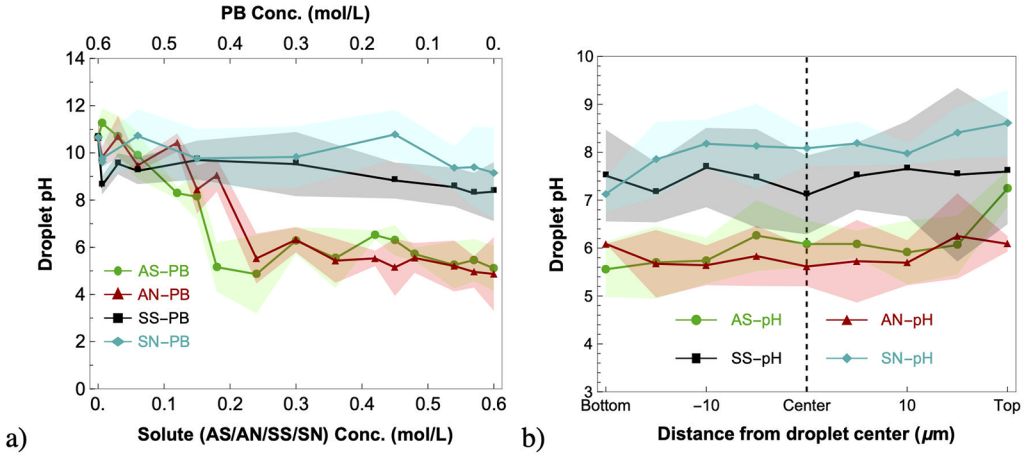

Figure 2. (a) Effects of an increasing amount of a second solute [ammonium sulfate (AS) or ammonium nitrate (AN) or sodium sulfate (SS) or sodium nitrate (SN)] and the concomitant decrease in phosphate buffer (PB) on the pH of PB droplets. The upper *x*-axis represents the PB concentration in the mixed solution and the lower *x*-axis represents the other solute in the mixture. The heights of the colored belts indicate the standard deviation of 20 replicate droplets at each concentration. (b) Mean pH measured for pure 0.6 M AS, SS, AN, and SN droplets at specific distances away from the droplet centroid.

Ammonium partitions throughout the droplet, except for a thin depletion layer,[58] and moves across the droplet with minimal restrictions,[56] thus the assumption of a homogeneous distribution of ammonium is reasonable. As a result, the hydronium distribution, which is at least partially dictated by the ammonium distribution, is more homogeneous in the ammonium droplets than in PB droplets. No apparent pH effect was observed, especially for increments in concentration, for either PB/AS or PB/AN droplets which suggests that the pH measured at 95% RH in this study may represent the droplet pH at other environmentally relevant RHs. Because the droplets in this study contained only salts, and ammonia gas partitioning was limited, the decrease in RH should only cause the droplet salt concentration to increase because of the loss of water.[2,59,60]

Atmospheric aerosols contain high ammonium sulfate concentrations (several ppb) and within the U.S. are usually reported to have fairly low pH ($\leq$2);[53] however, our results indicate that the pH of AS or AN droplets is in the range of 4−6. We attribute this discrepancy to two factors: (1) the simple composition of our AS droplets and (2) droplet size effects. Herein, the droplets consisted merely of stoichiometrically balanced ammonium and sulfate; however, atmospheric aerosols typically contain different cations, anions, and organics and have a higher sulfate concentration in the aerosol phase.[53,61,62] To address this complexity, sulfuric acid or hydrogen chloride were added to 1 M AS droplets. More acidic, environmentally relevant pH values (2.5 $\pm$ 0.8 for AS-H_2SO_4 droplets and 2.9 $\pm$ 0.9 for AS-HCl droplets) were achieved (Table S3). For fine-size aerosols (<2.5 μm), Ault et al. observed a trend of increasing particle acidity with a decrease in particle size. The pH of coarse-mode $(NH_4)_2SO_4$−H_2SO_4 aerosols was about 1−2 units higher than that of fine-mode aerosols.[63] Our droplets were 10−50 μm in diameter (i.e., the typical size range of mechanically generated aerosols[64]). No obvious size-related pH change was observed either here (Figure S4) or previously.[1]

Effect of Ammonium on the pH of PB Aerosol Droplets. To directly evaluate how ammonium affects the pH and ion distribution of PB droplets, the aerosol droplet composition was modified by systematically replacing PB with AS. As shown in Figure 2a, the measured pH of droplets decreased when the ammonium concentration (AS or AN) increased. The decrease in droplet pH with an increase in ammonium is similar to an acid−base titration. The droplet pH decreased within a narrow ammonium range of 0.12−0.24 M. The measured pH was ≈5 when the ammonium concentration was greater than 0.24 M. Such a pH decrease was not observed in bulk solution (Figure S7). SS-PB and SN-PB droplets were studied as controls, and the pH of these droplets decreased much less relative to AS- or AN-PB droplets when the concentration of SS and SN increased. The pH difference between PB droplets with high AS/AN concentration and PB droplets with high SS/SN concentration suggests that the presence of ammonium affects aerosol droplet pH and the ion distribution. The decrease in pH with the addition of ammonium in the AS- or AN-PB droplets suggests that the aforementioned heterogeneous distribution of phosphate anions is altered by ammonium. In contrast, sodium (in SN, SS) has a much weaker effect on the phosphate anion distribution. The pH of pure 0.6 M SN and SS droplets at their centroids was observed to be around 8. This pH value is lower than that of PB droplets but higher than that of bulk solutions of SN or SS or within ammonium droplets. Such a pH value indicates a slight propensity of hydronium to the air−water interface because of the heterogeneous distribution of ions in SN and SS droplets and the weaker interfacial preference of sodium relative to ammonium. The difference between ammonium and sodium is further discussed in the next section. 3D pH measurements of pure 0.6 M ammonium and sodium salt droplets were obtained to determine the pH variation and ion distribution across these droplets (Figure 2b). Consistently higher pH values were observed for sodium droplets than for ammonium droplets at all measured locations within a droplet. No obvious pH gradient was observed from the bottom to the top for either ammonium or sodium droplets. This result suggests a more homogenous ion distribution within these droplets relative to the PB droplets. We attribute the slightly higher pH near the droplet top-edge to the low signal-to-noise ratio.

As illustrated in Figure 1a, the variation in PB concentration did not reduce the pH below 10 until the PB concentration

https://dx.doi.org/10.1021/acs.est.0c07394
Environ. Sci. Technol. 2021, 55, 778−787

was <0.03 M. To better understand the pH change observed in AS-PB droplets, we virtually titrated 0.5 M PB and 0.01 M PB of pH = 7.4 and pH = 11 with AS using Visual MINTEQ ver. 3.1. In this process, the AS concentration was varied from 0 to 1 M using a 0.01 M step. For PB at pH = 7.4, which has an equivalent pH to the bulk PB applied in this study, an AS concentration that is 10× larger than that of PB was required to overcome the buffering capacity of PB. For PB with pH = 11, which simulates the pH at the PB centroid droplet, the solution pH decreases to ≈8.5 when the AS concentration was equivalent to the PB concentration. In contrast, in droplets, the pH exhibited an acute decrease to ≈5 under conditions where AS and PB have similar concentrations. The disagreement between these simulations for bulk solutions and the droplet measurements reinforces the idea that influences other than concentration (i.e., the aforementioned change in ion distribution due to interfacial preferences inside droplets) are introduced by ammonium addition.

The liquid-to-gas partitioning of ammonia was evaluated for the ammonium-PB droplets. According to our previous study, PB droplets exhibit a pH gradient of 8−11 from the exterior to the interior.[1] Before the sharp decrease in pH of a AS-PB droplet at an AS concentration <0.24 M, ammonia should be the predominant form of ammonium ion (high NH_3/NH_4^+ ratio) in the center of a PB droplet. However, the lower pH near the interface alters the NH_3/NH_4^+ ratio, resulting in an ammonium-dominated region near the droplet interface. Given the high solubility of ammonia in water and the decreasing NH_3/NH_4^+ ratio from the droplet centroid to the interface, the liquid-to-gas partitioning of ammonia may be suppressed in these ammonium-PB droplets. To experimentally evaluate ammonia partitioning, aluminum foil was used as a hydrophilic substrate for the collection of a thin film of aerosolized droplets. This thin film had a surface-to-volume ratio about 1/1000 of that of a droplet and thus can be regarded as a bulk solution post aerosolization. Equal volumes of 1 M AS were mixed with equal volumes of 1 M PB and 0.1 M PB, respectively, followed by pH nanoprobe addition. Gaseous ammonia formation during aerosolization and sample collection were evaluated according to the pH change. The measured pH before and after aerosolization was 7.3 ± 0.1 and 7.2 ± 0.5 for the 1 M PB mixture and 7.1 ± 0.1 and 6.9 ± 0.3 for the 0.1 M PB mixture. The insignificant pH difference in the solution before and after aerosolization indicated that ammonia degassing is negligible during sample collection and pH measurements. The 0.1 M PB mixture excluded the buffering effect from high-concentration PB. Therefore, the composition of the droplets in this study can be considered the same as the mixture suspension before aerosolization.

The difference between ammonium and sodium salts within droplets and the potential interfacial effect exerted by the pH nanoprobes were investigated by surface tension measurements of pendent droplets. Surface tension measurements can be related to surface excess through the Gibbs adsorption isotherm (GAI). In the GAI, the surface excess (Γ) is expressed as $\Gamma = -c/RT(d\gamma/dc) = -1/RT(d\gamma/d(\ln c))$. If the solution is not an ideal dilute system, the concentration (c) in the Gibbs equation is replaced by activity (a). Despite the existence of advanced thermodynamic models for multicomponent electrolyte solutions,[3,65] the GAI remains one of the best choices for qualitative analysis of droplet systems. As suggested previously, the size effect is weakened as the droplet size becomes larger than coarse mode aerosols; therefore, the correlation between surface tension and concentration may help determine whether the interface of the droplet experiences changes following addition of variable solutes and the nanoprobe, despite the fact that pendent droplets have a larger size relative to the micron droplets used within this study.

In the GAI, the dividing surface, which is an artificially defined virtual interface, can only be decided once and usually is where the solvent surface excess is zero.[66] To compare the measurement results, a 0.6 M PB droplet was taken as the reference state [Γ(0.6 M PB) = 0] because the majority of the multicomponent droplets in this study contained PB. The difference in surface tension ($\Delta\gamma$) caused by addition of the second solute into PB was quantified. As shown in Figure 3, $\Delta\gamma$ was linearly dependent on the AN and SN concentrations in the mixtures. The fitted slope for the AN−PB system is greater than that of the SN−PB mixture. A similar difference was observed between AS and SS (Figure S10). Importantly, the surface tensions of the AN−PB and SN−PB suspensions containing the pH nanoprobe did not significantly deviate from the measured AN−PB and SN−PB solution surface tensions for the same solution compositions, which indicated no quantitative impact of nanoprobe addition on the ion distribution.

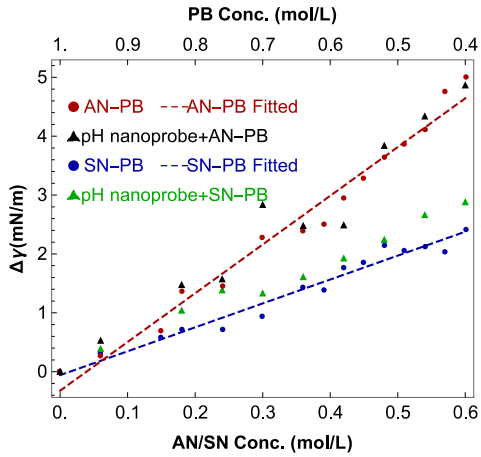

Figure 3. Surface tension of AN-PB and SN-PB mixture solutions with and without the pH nanoprobe. The triangles represent the mixture solutions with the pH nanoprobe. The y-axis denotes the surface tension difference between the mixture system and 1 M PB. The upper x-axis represents the PB concentration in the sample solution, and the lower x-axis represents the other salt in the solution.

According to the GAI, the higher slope for ammonium-PB droplets indicates a greater influence on droplet surface tension because of the addition of ammonium salts, which suggests a greater differential change in the ion distribution in ammonium-PB droplets with an increase in ammonium concentration. This result is consistent with the proposed ion distribution change in PB droplets relative to AS/AN droplets. The higher slope for ammonium-PB droplets also suggests that the overall surface excess of the ammonium-PB droplets was lower than that of sodium-PB droplets. The lower surface excess in ammonium-PB droplets denotes a greater ion depletion from the air−water interface. If the depleted ion is primarily $H_2PO_4^-$, then the higher surface tension change in the ammonium-PB droplets is consistent with their lower pH.

https://dx.doi.org/10.1021/acs.est.0c07394
Environ. Sci. Technol. 2021, 55, 778−787

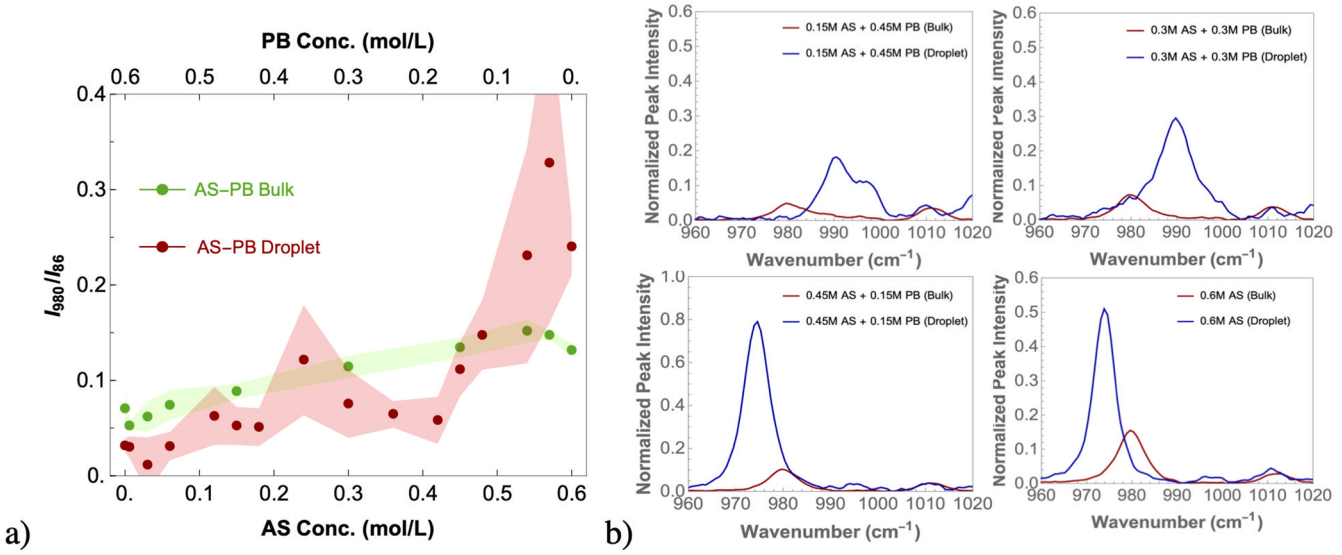

Figure 4. (a) Normalized peak intensity at ≈980 cm^{-1} (superposition of vibration mode of sulfate and phosphate) over the peak intensity at 86 cm^{-1} for AS-PB bulk solutions and AS-PB droplets, Raman spectra used for this graph had a grating of 300 g/mm; (b) high grating (1200 g/mm) SERS spectra of AS-PB bulk and AS-PB droplet at 980 cm^{-1} at four different representative compositions: (i) 0.25 M AS + 0.75 M PB; (ii) 0.5 M AS + 0.5 M PB; (iii) 0.75 M AS + 0.25 M PB; and (iv) 1 M AS. Each bulk solution spectrum is the average of triplicates and each droplet spectrum is the average of 6 SERS maps of 6 droplets (AS—ammonium sulfate, PB—phosphate buffer).

Ion Distribution in Ammonium-PB and Sodium-PB Droplets. The elevated pH observed in PB, SS, and SN droplets relative to their bulk solutions suggests sulfate or phosphate enrichment in the droplet centroid. Such enrichment was qualitatively observed via SERS (Figure 4a,b). The data were collected using the same protocol as used for the pH measurements. Our previous work has led to the development of an improved quantitative SERS method that normalizes analyte characteristic peaks to a low-wavenumber signal that reflects either electronic Raman scattering or surface-enhanced Raleigh scattering.[1,67] Accordingly, the amount of sulfate can be qualitatively determined by normalizing the characteristic sulfate symmetric stretch at 980 cm^{-1} to the aforementioned low-wavenumber band at 86 cm^{-1}.[67−69] We note that although the P−O stretch is in the vicinity of the S−O stretch (~985 cm^{-1}), the P−O stretch is generally weaker than that for S−O.[70,71] The relationship between the I_{980}/I_{86} peak ratio and the sulfate concentration for bulk solutions of AS−PB (Figure 4a) illustrates that the sulfate stretch generally correlates with concentration. Furthermore, the peak shifts illustrated in the four graphs in Figure 4b can be attributed to the superposition of the P−O and S−O stretches. The peak location changed with the variation in droplet composition. The measured 980/86 cm^{-1} peak ratio for droplets was higher than that of bulk solutions when the AS concentration was >0.45 M. The peak ratio represents the overall average of sulfate and phosphate in the droplet centroid. The higher peak ratio found within high-AS-concentration droplets suggested a higher number of sulfate and phosphate ions in the centroid of those droplets. A large standard deviation was found for high-AS-concentration droplets, which could be due to (1) variability across individual measured droplets and (2) spatial and temporal changes in ion distributions within droplets during measurement. Normalized SERS was applied to minimize the uncertainty from SERS measurements. The correlation found between normalized intensity and AS concentration in bulk solutions and the significantly increased normalized peak intensity in high-AS-concentration droplets support the idea of higher sulfate and phosphate concentrations at the droplet centroid.

High-resolution spectra (Figure 4b) were collected using a higher grating (1200 g/mm), and higher relative sulfate peak intensities were observed in all four droplet spectra. We note that we utilized the 1076 cm^{-1} peak of 4-MBA for signal normalization in Figure 4b because of the shorter spectral window available with this grating. The 4-MBA peak intensity should be proportional to the previously used low-wavenumber band intensity as 4-MBA is functionalized on AuNPs (Figure S11). Regular Raman spectra of AS-PB droplets without pH nanoprobes showed that the higher S−O stretch peak intensity in droplets coincided with SERS results (Figure S12). The consistently higher sulfate peak intensity found in the droplet centroid in both Raman and SERS spectra indicated that sulfate was enriched in the droplet centroid and the effect from the pH nanoprobe was negligible.

The pH difference observed between ammonium-PB droplets and sodium-PB droplets can be attributed to the different effects of ammonium and sodium cations in the droplet. Even though cationic effects are often regarded as less important than anionic effects,[49] the pH differences observed herein suggest that the local cation distribution affects the pH of micron-sized droplets. Because ammonium is a weak acid, the bulk solution pH of AS/AN is lower than that of SS/SN, and the pH of an AS/AN droplet is potentially lower than that of a SS/SN droplet. Furthermore, previous studies have observed that ammonium has a greater surface propensity relative to sodium in high-concentration systems such as in this study.[31,52,58] In droplets with high ammonium concentration, because of the "hydronium-like" structure of ammonium, as more ammonium partitions closer to the air/water interface, more hydronium is depleted from the air/water interface, thus neutralizing the high centroid pH of the PB droplets. As a result, the population of hydronium ions in the droplet centroid of an ammonium droplet is likely greater than the hydronium concentration in the sodium droplets, which causes

https://dx.doi.org/10.1021/acs.est.0c07394
Environ. Sci. Technol. 2021, 55, 778−787

the pH at the centroid of AS and AN droplets to be lower than that in SN and SS droplets.

Implications. In this study, pH effects arising from changes in solute concentration and droplet composition were investigated. The stable pH observed at different solute concentrations indicated that the measured pH in this study may represent droplet pH at environmentally relevant RH values before efflorescence. Ammonium salts (AS, AN) and sodium salts (SS, SN) were added into PB droplets to quantify their influence on droplet pH. When the ammonium content was increased in ammonium-PB droplets, the centroid pH of the droplets decreased from basic (≈11) and converged with the pH of the bulk solution (≈5.5). Such a pH change was attributed to a change in ion distribution caused by ammonium addition. The higher pH in the original PB droplets compared to their bulk solution was attributed to the heterogeneous ion distribution. Among all ions, except for hydronium, ammonium has the highest affinity toward the air−water interface and moves unhindered in water.[31,56] As the fraction of ammonium increased in the PB droplets, the ions in droplets become more homogeneously distributed. This finding suggests that the ion distribution within a droplet is largely affected by its composition and that this affects the measured pH. The more homogeneous ion distribution in ammonium droplets illustrates why thermodynamic models are valid for atmospheric aerosol pH prediction when considering an ensemble of aerosols and gas-phase partitioning. However, model-predicted values can only represent an average of a collection of droplets, while individual aerosol droplet pH values may vary considerably from the predicted values because of the different ion distributions between droplets and the dynamic nature of individual aerosol droplets (e.g., the semi-volatile nature of water[72]). We determined that ammonium partitioning was negligible under the conditions of this study; however, under different conditions (e.g., concentration, RH, and so on), ammonium partitioning may need to be re-evaluated. The assumption of spatially homogeneous composition cannot always be made when considering droplet interactions with the surrounding environment. The application of SERS-active pH nanoprobes in micron-scale systems with high interfacial area, such as atmospheric aerosols and indoor surface films, may provide information beyond pH distribution. The pH distribution can be regarded as an indicator of ion distributions and their interfacial preference that may correlate with heterogeneous interfacial processes (e.g., surface sorption,[73] evaporation,[56] and so forth).

■ ASSOCIATED CONTENT

Supporting Information

The Supporting Information is available free of charge at https://pubs.acs.org/doi/10.1021/acs.est.0c07394.

DLS measurement results, E-AIM calculated results, pH values, UV−vis spectra, observation and optical image of 1M PB and 1M AS droplets, size distribution of droplets, SERS spectra, comparison of pH, measured pH of bulk solutions, pH calculated by Visual MINTEQ, phosphate buffer pH, surface tension of AS-PB and SS-PB mixtures, peak ratio at different concentrations, and Raman spectra (PDF)

■ AUTHOR INFORMATION

Corresponding Author

Peter J. Vikesland − *Department of Civil and Environmental Engineering, Virginia Tech, Blacksburg, Virginia 24061, United States; Virginia Tech Institute of Critical Technology and Applied Science (ICTAS) Sustainable Nanotechnology Center, Blacksburg, Virginia 24061, United States;* orcid.org/0000-0003-2654-5132; Email: pvikes@vt.edu

Authors

Qishen Huang − *Department of Civil and Environmental Engineering, Virginia Tech, Blacksburg, Virginia 24061, United States; Virginia Tech Institute of Critical Technology and Applied Science (ICTAS) Sustainable Nanotechnology Center, Blacksburg, Virginia 24061, United States*

Haoran Wei − *Department of Civil and Environmental Engineering, University of Wisconsin-Madison, Madison, Wisconsin 53706, United States;* orcid.org/0000-0001-6871-0891

Linsey C. Marr − *Department of Civil and Environmental Engineering, Virginia Tech, Blacksburg, Virginia 24061, United States; Virginia Tech Institute of Critical Technology and Applied Science (ICTAS) Sustainable Nanotechnology Center, Blacksburg, Virginia 24061, United States;* orcid.org/0000-0003-3628-6891

Complete contact information is available at: https://pubs.acs.org/10.1021/acs.est.0c07394

Notes

The authors declare no competing financial interest.

■ ACKNOWLEDGMENTS

We thank Dr. Weinan Leng for assistance with the Raman experiments. This research was supported by the National Science Foundation (CBET-1705653). Laboratory and instrumentation support was provided by NanoEarth a node of the NSF supported NNCI (NSF award number #1542100). Additional support was provided by the Sustainable Nanotechnology Interdisciplinary Graduate Program (VTSuN IGEP) funded by the Virginia Tech Graduate School.

■ REFERENCES

(1) Wei, H.; Vejerano, E. P.; Leng, W.; Huang, Q.; Willner, M. R.; Marr, L. C.; Vikesland, P. J. Aerosol Microdroplets Exhibit a Stable pH Gradient. *Proc. Natl. Acad. Sci.* **2018**, *115*, 7272−7277.

(2) Köhler, H. The Nucleus in and the Growth of Hygroscopic Droplets. *Trans. Faraday Soc.* **1936**, *32*, 1152−1161.

(3) Pegram, L. M.; Record, M. T. Partitioning of Atmospherically Relevant Ions between Bulk Water and the Water/Vapor Interface. *Proc. Natl. Acad. Sci. U.S.A.* **2006**, *103*, 14278−14281.

(4) Ault, A. P.; Axson, J. L. Atmospheric Aerosol Chemistry: Spectroscopic and Microscopic Advances. *Anal. Chem.* **2017**, *89*, 430−452.

(5) Seinfeld, J. H.; Spyros, N. P. *Atmospheric Chemistry and Physics: From Air Pollution to Climate Change*, 3rd ed.; John Wiley & Sons: NJ, 2016.

(6) Fang, T.; Guo, H.; Zeng, L.; Verma, V.; Nenes, A.; Weber, R. J. Highly Acidic Ambient Particles, Soluble Metals, and Oxidative Potential: A Link between Sulfate and Aerosol Toxicity. *Environ. Sci. Technol.* **2017**, *51*, 2611−2620.

(7) Marr, L. C.; Tang, J. W.; Van Mullekom, J.; Lakdawala, S. S. Mechanistic Insights into the Effect of Humidity on Airborne Influenza Virus Survival, Transmission and Incidence. *J. R. Soc. Interface* **2019**, *16*, 20180298.

(8) Yang, W.; Marr, L. C. Mechanisms by Which Ambient Humidity May Affect Viruses in Aerosols. *Appl. Environ. Microbiol.* **2012**, *78*, 6781−6788.
(9) Freedman, M. A.; Ott, E.-J. E.; Marak, K. E. Role of pH in Aerosol Processes and Measurement Challenges. *J. Phys. Chem. A* **2019**, *123*, 1275−1284.
(10) Pye, H. O. T.; Nenes, A.; Alexander, B.; Ault, A. P.; Barth, M. C.; Clegg, S. L.; Collett, J. L., Jr; Fahey, K. M.; Hennigan, C. J.; Herrmann, H.; Kanakidou, M.; Kelly, J. T.; Ku, I.-T.; Mcneill, V. F.; Riemer, N.; Schaefer, T.; Shi, G.; Tilgner, A.; Walker, J. T.; Wang, T.; Weber, R.; Xing, J.; Zaveri, R. A.; Zuend, A. The Acidity of Atmospheric Particles and Clouds. *Atmos. Chem. Phys. Discuss.* **2019**, *20*, 4809.
(11) Chameides, W. L. The Photochemistry of a Remote Marine Stratiform Cloud. *J. Geophys. Res.* **1984**, *89*, 4739−4755.
(12) Young, A. H.; Keene, W. C.; Pszenny, A. A. P.; Sander, R.; Thornton, J. A.; Riedel, T. P.; Maben, J. R. Phase Partitioning of Soluble Trace Gases with Size-Resolved Aerosols in near-Surface Continental Air over Northern Colorado, USA, during Winter. *J. Geophys. Res. Atmos.* **2013**, *118*, 9414−9427.
(13) Farmer, D. K.; Cappa, C. D.; Kreidenweis, S. M. Atmospheric Processes and Their Controlling Influence on Cloud Condensation Nuclei Activity. *Chem. Rev.* **2015**, *115*, 4199−4217.
(14) DuBois, R. M.; Zaraket, H.; Reddivari, M.; Heath, R. J.; White, S. W.; Russell, C. J. Acid Stability of the Hemagglutinin Protein Regulates H5N1 Influenza Virus Pathogenicity. *PLoS Pathog.* **2011**, *7*, No. e1002398.
(15) Losey, D. J.; Parker, R. G.; Freedman, M. A. pH Dependence of Liquid-Liquid Phase Separation in Organic Aerosol. *J. Phys. Chem. Lett.* **2016**, *7*, 3861−3865.
(16) Ault, A. P.; Guasco, T. L.; Ryder, O. S.; Baltrusaitis, J.; Cuadra-Rodriguez, L. A.; Collins, D. B.; Ruppel, M. J.; Bertram, T. H.; Prather, K. A.; Grassian, V. H. Inside versus Outside: Ion Redistribution in Nitric Acid Reacted Sea Spray Aerosol Particles as Determined by Single Particle Analysis. *J. Am. Chem. Soc.* **2013**, *135*, 14528−14531.
(17) Hallquist, M.; Wenger, J. C.; Baltensperger, U.; Rudich, Y.; Simpson, D.; Claeys, M.; Dommen, J.; Donahue, N. M.; George, C.; Goldstein, A. H.; Hamilton, J. F.; Herrmann, H.; Hoffmann, T.; Iinuma, Y.; Jang, M.; Jenkin, M. E.; Jimenez, J. L.; Kiendler-Scharr, A.; Maenhaut, W.; McFiggans, G.; Mentel, T. F.; Monod, A.; Prévôt, A. S. H.; Seinfeld, J. H.; Surratt, J. D.; Szmigielski, R.; Wildt, J. The Formation, Properties and Impact of Secondary Organic Aerosol: Current and Emerging Issues. *Atmos. Chem. Phys.* **2009**, *9*, 5155−5236.
(18) Jimenez, J. L.; Canagaratna, M. R.; Donahue, N. M.; Prevot, A. S. H.; Zhang, Q.; Kroll, J. H.; DeCarlo, P. F.; Allan, J. D.; Coe, H.; Ng, N. L.; Aiken, A. C.; Docherty, K. S.; Ulbrich, I. M.; Grieshop, A. P.; Robinson, A. L.; Duplissy, J.; Smith, J. D.; Wilson, K. R.; Lanz, V. A.; Hueglin, C.; Sun, Y. L.; Tian, J.; Laaksonen, A.; Raatikainen, T.; Rautiainen, J.; Vaattovaara, P.; Ehn, M.; Kulmala, M.; Tomlinson, J. M.; Collins, D. R.; Cubison, M. J.; Dunlea, J.; Huffman, J. A.; Onasch, T. B.; Alfarra, M. R.; Williams, P. I.; Bower, K.; Kondo, Y.; Schneider, J.; Drewnick, F.; Borrmann, S.; Weimer, S.; Demerjian, K.; Salcedo, D.; Cottrell, L.; Griffin, R.; Takami, A.; Miyoshi, T.; Hatakeyama, S.; Shimono, A.; Sun, J. Y.; Zhang, Y. M.; Dzepina, K.; Kimmel, J. R.; Sueper, D.; Jayne, J. T.; Herndon, S. C.; Trimborn, A. M.; Williams, L. R.; Wood, E. C.; Middlebrook, A. M.; Kolb, C. E.; Baltensperger, U.; Worsnop, D. R. Evolution of Organic Aerosols in the Atmosphere. *Science* **2009**, *326*, 1525−1529.
(19) McFiggans, G.; Artaxo, P.; Baltensperger, U.; Coe, H.; Facchini, M. C.; Feingold, G.; Fuzzi, S.; Gysel, M.; Laaksonen, A.; Lohmann, U.; Mentel, T. F.; Murphy, D. M.; O'Dowd, C. D.; Snider, J. R.; Weingartner, E. The Effect of Physical and Chemical Aerosol Properties on Warm Cloud Droplet Activation. *Atmos. Chem. Phys.* **2006**, *6*, 2593−2649.
(20) Zhang, R. Getting to the Critical Nucleus of Aerosol Formation. *Science* **2010**, *328*, 1365−1366.
(21) Chen, M.; Titcombe, M.; Jiang, J.; Jen, C.; Kuang, C.; Fischer, M. L.; Eisele, F. L.; Siepmann, J. I.; Hanson, D. R.; Zhao, J.; McMurry, P. H. Acid-Base Chemical Reaction Model for Nucleation Rates in the Polluted Atmospheric Boundary Layer. *Proc. Natl. Acad. Sci.* **2013**, *1527*, 647−650.
(22) Kirkby, J.; Curtius, J.; Almeida, J.; Dunne, E.; Duplissy, J.; Ehrhart, S.; Franchin, A.; Gagné, S.; Ickes, L.; Kürten, A.; Kupc, A.; Metzger, A.; Riccobono, F.; Rondo, L.; Schobesberger, S.; Tsagkogeorgas, G.; Wimmer, D.; Amorim, A.; Bianchi, F.; Breitenlechner, M.; David, A.; Dommen, J.; Downard, A.; Ehn, M.; Flagan, R. C.; Haider, S.; Hansel, A.; Hauser, D.; Jud, W.; Junninen, H.; Kreissl, F.; Kvashin, A.; Laaksonen, A.; Lehtipalo, K.; Lima, J.; Lovejoy, E. R.; Makhmutov, V.; Mathot, S.; Mikkilä, J.; Minginette, P.; Mogo, S.; Nieminen, T.; Onnela, A.; Pereira, P.; Petäjä, T.; Schnitzhofer, R.; Seinfeld, J. H.; Sipilä, M.; Stozhkov, Y.; Stratmann, F.; Tomé, A.; Vanhanen, J.; Viisanen, Y.; Vrtala, A.; Wagner, P. E.; Walther, H.; Weingartner, E.; Wex, H.; Winkler, P. M.; Carslaw, K. S.; Worsnop, D. R.; Baltensperger, U.; Kulmala, M. Role of Sulphuric Acid, Ammonia and Galactic Cosmic Rays in Atmospheric Aerosol Nucleation. *Nature* **2011**, *476*, 429−433.
(23) Townsend, T. M.; Allanic, A.; Noonan, C.; Sodeau, J. R. Characterization of Sulfurous Acid, Sulfite, and Bisulfite Aerosol Systems. *J. Phys. Chem. A* **2012**, *116*, 4035−4046.
(24) Behera, S. N.; Sharma, M.; Aneja, V. P.; Balasubramanian, R. Ammonia in the Atmosphere: A Review on Emission Sources, Atmospheric Chemistry and Deposition on Terrestrial Bodies. *Environ. Sci. Pollut. Res.* **2013**, *20*, 8092−8131.
(25) Zhang, T.; Brantley, S. L.; Verreault, D.; Dhankani, R.; Corcelli, S. A.; Allen, H. C. Effect of pH and Salt on Surface pK_a of Phosphatidic Acid Monolayers. *Langmuir* **2018**, *34*, 530−539.
(26) Mondal, S.; Acharya, S.; Biswas, R.; Bagchi, B.; Zare, R. N. Enhancement of Reaction Rate in Small-Sized Droplets: A Combined Analytical and Simulation Study. *J. Chem. Phys.* **2018**, *148*, 244704.
(27) Gao, D.; Jin, F.; Yan, X.; Zare, R. N. Selective Synthesis in Microdroplets of 2-Phenyl-2,3-Dihydrophthalazine-1,4-Dione from Phenyl Hydrazine with Phthalic Anhydride or Phthalic Acid. *Chem.—Eur. J.* **2019**, *25*, 1466−1471.
(28) Liu, D.; Ma, G.; Levering, L. M.; Allen, H. C. Vibrational Spectroscopy of Aqueous Sodium Halide Solutions and Air−Liquid Interfaces: Observation of Increased Interfacial Depth. *J. Phys. Chem. B* **2004**, *108*, 2252−2260.
(29) Wick, C. D. A comparison of sodium and hydrogen halides at the air-water interface. *J. Chem. Phys.* **2017**, *147*, 161703.
(30) Dang, L. X. Solvation of the Hydronium Ion at the Water Liquid/Vapor Interface. *J. Chem. Phys.* **2003**, *119*, 6351−6353.
(31) Hua, W.; Verreault, D.; Allen, H. C. Relative Order of Sulfuric Acid, Bisulfate, Hydronium, and Cations at the Air-Water Interface. *J. Am. Chem. Soc.* **2015**, *137*, 13920−13926.
(32) Guo, H.; Xu, L.; Bougiatioti, A.; Cerully, K. M.; Capps, S. L.; Hite, J. R.; Carlton, A. G.; Lee, S.-H.; Bergin, M. H.; Ng, N. L.; Nenes, A.; Weber, R. J. Fine-Particle Water and pH in the Southeastern United States. *Atmos. Chem. Phys.* **2015**, *15*, 5211−5228.
(33) Hennigan, C. J.; Izumi, J.; Sullivan, A. P.; Weber, R. J.; Nenes, A. A Critical Evaluation of Proxy Methods Used to Estimate the Acidity of Atmospheric Particles. *Atmos. Chem. Phys.* **2015**, *15*, 2775−2790.
(34) Wexler, A. S.; Clegg, S. L. Atmospheric aerosol models for systems including the ions H+, NH4+, Na+, SO42−, NO3−, Cl−, Br−, and H2O. *J. Geophys. Res. Atmos.* **2002**, *107*. DOI: 10.1029/2001JD000451.
(35) Fountoukis, C.; Nenes, A. ISORROPIA II: a computationally efficient thermodynamic equilibrium model for K+−Ca2+−Mg2+−NH4+−Na+−SO42−−NO3−−Cl−−H2O. *Atmos. Chem. Phys.* **2007**, *7*, 4639−4659.
(36) Pöschl, U. Atmospheric Aerosols: Composition, Transformation, Climate and Health Effects. *Angew. Chem., Int. Ed.* **2005**, *44*, 7520−7540.
(37) Nie, W.; Ding, A.; Wang, T.; Kerminen, V.-M.; George, C.; Xue, L.; Wang, W.; Zhang, Q.; Petäjä, T.; Qi, X.; Gao, X.; Wang, X.;

Yang, X.; Fu, C.; Kulmala, M. Polluted Dust Promotes New Particle Formation and Growth. *Sci. Rep.* **2014**, *4*, 6634.
(38) Ault, A. P.; Zhao, D.; Ebben, C. J.; Tauber, M. J.; Geiger, F. M.; Prather, K. A.; Grassian, V. H. Raman Microspectroscopy and Vibrational Sum Frequency Generation Spectroscopy as Probes of the Bulk and Surface Compositions of Size-Resolved Sea Spray Aerosol Particles. *Phys. Chem. Chem. Phys.* **2013**, *15*, 6206.
(39) Rindelaub, J. D.; Craig, R. L.; Nandy, L.; Bondy, A. L.; Dutcher, C. S.; Shepson, P. B.; Ault, A. P. Direct Measurement of pH in Individual Particles via Raman Microspectroscopy and Variation in Acidity with Relative Humidity. *J. Phys. Chem. A* **2016**, *120*, 911−917.
(40) Craig, R. L.; Nandy, L.; Axson, J. L.; Dutcher, C. S.; Ault, A. P. Spectroscopic Determination of Aerosol pH from Acid-Base Equilibria in Inorganic, Organic, and Mixed Systems. *J. Phys. Chem. A* **2017**, *121*, 5690−5699.
(41) Leng, W.; Vikesland, P. J. MGITC Facilitated Formation of AuNP Multimers. *Langmuir* **2014**, *30*, 8342−8349.
(42) Wei, H.; Willner, M. R.; Marr, L. C.; Vikesland, P. J. Highly Stable SERS pH Nanoprobes Produced by Co-Solvent Controlled AuNP Aggregation. *Analyst* **2016**, *141*, 5159−5169.
(43) Frens, G. Controlled Nucleation for the Regulation of the Particle Size in Monodisperse Gold Suspensions. *Nat. Phys. Sci.* **1973**, *241*, 20−22.
(44) Petters, M. D.; Kreidenweis, S. M. A single parameter representation of hygroscopic growth and cloud condensation nucleus activity - Part 2: Including solubility; **2008**; Vol. *8*, 6273. DOI: 10.5194/acp-8-6273-2008.
(45) Lewis, E. R. An Examination of Köhler Theory Resulting in an Accurate Expression for the Equilibrium Radius Ratio of a Hygroscopic Aerosol Particle Valid up to and Including Relative Humidity 100%. *J. Geophys. Res. Atmos.* **2008**, *113*, D03205.
(46) Clegg, S. L.; Brimblecombe, P.; Wexler, A. S. Thermodynamic Model of the System H+−NH4+−Na+−SO42-−NO3-−Cl-−H2O at 298.15 K. *J. Phys. Chem. A* **1998**, *102*, 2155−2171.
(47) Ho, C.-H.; Lee, S. SERS and DFT Investigation of the Adsorption Behavior of 4-Mercaptobenzoic Acid on Silver Colloids. *Colloids Surf., A* **2015**, *474*, 29−35.
(48) Tissandier, M. D.; Cowen, K. A.; Feng, W. Y.; Gundlach, E.; Cohen, M. H.; Earhart, A. D.; Coe, J. V.; Tuttle, T. R. The Proton's Absolute Aqueous Enthalpy and Gibbs Free Energy of Solvation from Cluster-Ion Solvation Data. *J. Phys. Chem. A* **1998**, *102*, 7787−7794.
(49) Jungwirth, P.; Tobias, D. J. Specific Ion Effects at the Air/Water Interface. *Chem. Rev.* **2006**, *106*, 1259−1281.
(50) Atkins, P.; de Paula, J.; Keeler, J. *Atkins' Physical Chemistry*, 11th ed.; Oxford University Press, 2018.
(51) Wang, X.-B.; Yang, X.; Nicholas, J. B.; Wang, L.-S. Bulk-like Features in the Photoemission Spectra of Hydrated Doubly Charged Anion Clusters. *Science* **2001**, *294*, 1322−1325.
(52) Gopalakrishnan, S.; Jungwirth, P.; Tobias, D. J.; Allen, H. C. Air−Liquid Interfaces of Aqueous Solutions Containing Ammonium and Sulfate: Spectroscopic and Molecular Dynamics Studies. *J. Phys. Chem. B* **2005**, *109*, 8861−8872.
(53) Weber, R. J.; Guo, H.; Russell, A. G.; Nenes, A. High Aerosol Acidity despite Declining Atmospheric Sulfate Concentrations over the Past 15 Years. *Nat. Geosci.* **2016**, *9*, 282−285.
(54) Aydin, F.; Zhan, C.; Ritt, C.; Epsztein, R.; Elimelech, M.; Schwegler, E.; Pham, T. A. Similarities and Differences between Potassium and Ammonium Ions in Liquid Water: A First-Principles Study. *Phys. Chem. Chem. Phys.* **2020**, *22*, 2540−2548.
(55) Marcus, Y. Ionic Radii in Aqueous Solutions. *Chem. Rev.* **1988**, *88*, 1475−1498.
(56) Caleman, C.; Van Der Spoel, D. Evaporation from Water Clusters Containing Singly Charged Ions. *Phys. Chem. Chem. Phys.* **2007**, *9*, 5105−5111.
(57) Iyengar, S. S.; Day, T. J. F.; Voth, G. A. On the Amphiphilic Behavior of the Hydrated Proton: An Ab Initio Molecular Dynamics Study. *Int. J. Mass Spectrom.* **2005**, *241*, 197−204.
(58) Hua, W.; Jubb, A. M.; Allen, H. C. Electric Field Reversal of Na2SO4, (NH4)2SO4, and Na2CO3 Relative to CaCl2 and NaCl at the Air/Aqueous Interface Revealed by Heterodyne Detected Phase-Sensitive Sum Frequency. *J. Phys. Chem. Lett.* **2011**, *2*, 2515−2520.
(59) Walker, J. S.; Wills, J. B.; Reid, J. P.; Wang, L.; Topping, D. O.; Butler, J. R.; Zhang, Y.-H. Direct Comparison of the Hygroscopic Properties of Ammonium Sulfate and Sodium Chloride Aerosol at Relative Humidities Approaching Saturation. *J. Phys. Chem. A* **2010**, *114*, 12682−12691.
(60) Peng, C.; Jing, B.; Guo, Y.-C.; Zhang, Y.-H.; Ge, M.-F. Hygroscopic Behavior of Multicomponent Aerosols Involving NaCl and Dicarboxylic Acids. *J. Phys. Chem. A* **2016**, *120*, 1029−1038.
(61) Guo, H.; Nenes, A.; Weber, R. J. The Underappreciated Role of Nonvolatile Cations in Aerosol Ammonium-Sulfate Molar Ratios. *Atmos. Chem. Phys.* **2018**, *18*, 17307−17323.
(62) Wang, G.; Zhang, R.; Gomez, M. E.; Yang, L.; Levy Zamora, M.; Hu, M.; Lin, Y.; Peng, J.; Guo, S.; Meng, J.; Li, J.; Cheng, C.; Hu, T.; Ren, Y.; Wang, Y.; Gao, J.; Cao, J.; An, Z.; Zhou, W.; Li, G.; Wang, J.; Tian, P.; Marrero-Ortiz, W.; Secrest, J.; Du, Z.; Zheng, J.; Shang, D.; Zeng, L.; Shao, M.; Wang, W.; Huang, Y.; Wang, Y.; Zhu, Y.; Li, Y.; Hu, J.; Pan, B.; Cai, L.; Cheng, Y.; Ji, Y.; Zhang, F.; Rosenfeld, D.; Liss, P. S.; Duce, R. A.; Kolb, C. E.; Molina, M. J. Persistent Sulfate Formation from London Fog to Chinese Haze. *Proc. Natl. Acad. Sci. U.S.A.* **2016**, *113*, 13630−13635.
(63) Craig, R. L.; Peterson, P. K.; Nandy, L.; Lei, Z.; Hossain, M. A.; Camarena, S.; Dodson, R. A.; Cook, R. D.; Dutcher, C. S.; Ault, A. P. Direct Determination of Aerosol pH: Size-Resolved Measurements of Submicrometer and Supermicrometer Aqueous Particles. *Anal. Chem.* **2018**, *90*, 11232.
(64) USEPA. *Air Quality Criteria for Particulate Matter*, 2004.
(65) Dutcher, C. S.; Wexler, A. S.; Clegg, S. L. Surface Tensions of Inorganic Multicomponent Aqueous Electrolyte Solutions and Melts. *J. Phys. Chem. A* **2010**, *114*, 12216−12230.
(66) Tuckermann, R. Surface Tension of Aqueous Solutions of Water-Soluble Organic and Inorganic Compounds. *Atmos. Environ.* **2007**, *41*, 6265−6275.
(67) Wei, H.; Leng, W.; Song, J.; Willner, M. R.; Marr, L. C.; Zhou, W.; Vikesland, P. J. Improved Quantitative SERS Enabled by Surface Plasmon Enhanced Elastic Light Scattering. *Anal. Chem.* **2018**, *90*, 3227−3237.
(68) Venkateswarlu, P.; Bist, H. D.; Jain, Y. S. Laser Excited Raman Spectrum of Ammonium Sulfate Single Crystal. *J. Raman Spectrosc.* **1975**, *3*, 143−151.
(69) Zhang, Y.-H.; Chan, C. K. Understanding the Hygroscopic Properties of Supersaturated Droplets of Metal and Ammonium Sulfate Solutions Using Raman Spectroscopy. *J. Phys. Chem. A* **2002**, *106*, 285−292.
(70) Šoptrajanov, B.; Stefov, V.; Kuzmanovski, I.; Jovanovski, G. Fourier Transform Infrared and Raman Spectra of Manganese Hydrogenphosphate Trihydrate. *J. Mol. Struct.* **1999**, *482*−*483*, 103−107.
(71) Degen, I. A.; Newman, G. A. Raman Spectra of Inorganic Ions. *Spectrochim. Acta, Part A* **1993**, *49*, 859−887.
(72) Kim, Y. P.; Seinfeld, J. H.; Saxena, P. Atmospheric Gas-Aerosol Equilibrium I. Thermodynamic Model. *Aerosol Sci. Technol.* **1993**, *19*, 157−181.
(73) Ongwandee, M.; Morrison, G. C. Influence of Ammonia and Carbon Dioxide on the Sorption of a Basic Organic Pollutant to Carpet and Latex-Painted Gypsum Board. *Environ. Sci. Technol.* **2008**, *42*, 5415−5420.

https://dx.doi.org/10.1021/acs.est.0c07394
Environ. Sci. Technol. 2021, 55, 778−787